Hindawi
Complexity
Volume 2022, Article ID 1250489, 18 pages
https://doi.org/10.1155/2022/1250489

WILEY | Hindawi

Research Article

Development of a Family of Chaotic Systems with Infinite Equilibria and Its Application for Image Encryption

Xiaofeng Li, Yulong Bai, Weishuan Pan, Di Wang, and Yong-Jie Ma

College of Physics and Electrical Engineering, Northwest Normal University, Lanzhou, China

Correspondence should be addressed to Yulong Bai; baiyulong@nwnu.edu.cn

Received 10 November 2021; Revised 4 January 2022; Accepted 23 February 2022; Published 30 March 2022

Academic Editor: Rosa M. Lopez Gutierrez

Copyright © 2022 Xiaofeng Li et al. This is an open access article distributed under the Creative Commons Attribution License, which permits unrestricted use, distribution, and reproduction in any medium, provided the original work is properly cited.

Fourth-order autonomous nonlinear differential equations can exhibit chaotic properties. In this study, we propose a family of fourth-order chaotic systems with infinite equilibrium points whose equilibria form closed curves of different shapes. First, the phase diagrams and Lyapunov exponents (LEs) of the system family are simulated. The results show that the system family has complex phase diagrams and dynamic behaviors. Simulation analysis of the Poincarè mapping and bifurcation diagrams shows that the system has chaotic characteristics. The circuit simulation model is constructed and simulated in Multisim. The circuit simulation results coincide with the numerical simulation results, which verifies the circuit feasibility of the system. Then, based on Lyapunov stability theory and the adaptive control method, the synchronous control of the system with infinite equilibria is designed. Numerical simulation results verify that the system synchronization with the adaptive control method is well. Finally, the synchronous drive system is used for image encryption, the response system is used for decryption, and color image encryption is realized by combining deoxyribonucleic acid (DNA) coding and operating rules. Therefore, this study not only enriched the research on infinite equilibria chaotic systems but also further expanded secure communication technology by combining chaotic synchronization control and DNA coding in image encryption.

1. Introduction

The study of chaotic systems has gradually become an important part of nonlinear dynamics since 1963 when Professor Lorenz proposed the classic Lorenz system [1]. Different characteristics have been identified in different chaotic systems, such as multi-scroll chaotic oscillators [2], fractional-order chaotic systems [3], three-dimensional chaotic systems [4], and chaotic systems with infinite equilibria [5]. Moreover, the complex dynamic characteristics of chaotic systems can be applied to audio encryption technology [6], image watermarking technology [7], chaotic mask communication [8], and other fields. As the research on chaotic systems has deepened, chaotic systems with infinite equilibrium points have gained attention and the analysis of their complex dynamic behavior has become a representative research direction.

Recently, investigating infinite equilibrium points in chaotic systems has attracted the attention of many researchers. In 2015, Gotthans et al. [9] proposed a new class of three-dimensional chaotic system, by analyzing two cases in which the system has infinite equilibrium points and constitutes a circle and a square, respectively. Later, the heart-shaped equilibria chaotic system proposed by Pham et al. [5], the pear-shaped equilibria chaotic system proposed by Aceng et al. [10], and the cloud-shaped curve of the equilibrium points chaotic system proposed by Vaidyanathan et al. [11], all promoted the rapid development of three-dimensional infinite equilibria chaotic system. In 2019, Huynh et al. [12] proposed a new four-dimensional memristor chaotic system with a series of equilibrium points and analyzed the stability interval of a series of equilibrium points. Subsequently, Yang et al. [13] proposed a four-dimensional chaotic system with a boomerang-like equilibrium based on Mobayen's [14] three-dimensional infinite equilibria chaotic system. Infinite equilibria chaotic systems can show complex dynamic characteristics. However, there are few discussions on the application of chaotic systems with infinite equilibria.

The applications of chaotic system mainly includes the following topics: weak signal detection [15], image

encryption [13, 16], data encryption [17], voice encryption [14], and chaotic system control [15, 18, 19]. Among these topics, image encryption and the synchronous control of the chaotic systems are still hot topics. There are many research studies on the image encryption of chaotic systems. For example, a double-channel image encryption/decryption algorithm based on neural networks and chaos [20] was designed; Huang et al. [21] proposed a parallel image encryption algorithm based on compressed sensing, which combines chaotic systems. Previous researchers have also studied image encryption algorithms based on DNA coding. Zhang and Liu [22] proposed different DNA coding and decoding rules based on generated chaotic sequences. Wang et al. [16] combined a chaotic system with DNA sequence operations to realize image encryption/decryption.

There are many methods for the synchronization and control of chaotic systems, such as active control, adaptive control, and sliding mode control. Based on the proposed Chua's circuit study, Li and Bo [15] realized a weak signal detection method via chaotic synchronization. Changbiao et al. [23] not only completed the signal tracking of the proposed unified chaotic system by designing an adaptive synovial controller but also realized the synchronous control of different structures. Fu et al. [24] have implemented an encryption algorithm and the double-chaotic system (the chaos synchronization between two chaotic systems). González-Zapata et al. [25] proposed the synchronization of chaotic artificial neurons and its application to secure image transmission. Ahmad et al. [26] proposed the application of multi-switch synchronization control system in secure communication, and Luo et al. [27] applied the multi-switch synchronization control of a memristor chaotic system in image encryption. However, this literature does not involve the keys and the coding is simple; therefore, we can improve the security of the encryption algorithm based on these two points.

The main works of this study are as follows:

(1) A family of chaotic systems with unique characteristics, which have closed equilibria with different curves, is proposed.

(2) An adaptive controller is designed. According to Lyapunov stability theory, master and slave systems can be synchronized and the synchronization effect works well.

(3) An image encryption/decryption algorithm is designed. An adaptive controller and DNA coding/encoding are selected to achieve the security requirements of encryption.

The remainder of this study is organized as follows: Section 2 proposes a class of chaotic systems with unique characteristics. Section 3 describes the phase portraits and dynamical analysis of the selected chaotic system, in which parameter k is 2. In Section 4, a circuital implementation of the new chaotic system is reported. In Section 5, the results for the synchronization of the chaotic system are derived via parameter adaptive control. Section 6 describes image encryption via the synchronization of the chaotic system as an engineering application of our work. Section 7 provides a brief discussion. Section 8 draws the main conclusions.

2. A Family of Chaotic Systems with Infinite Equilibria

The chaotic system proposed in reference [9] is shown in equation (1), where $g_1(x, y, z) = ay + by^2 + xz$ and $g_2(x, y, z) = x^2 + y^2$. The simulated phase diagram is shown in Figure 1, when $a = 5$, $b = 3$, and the initial conditions $(x_0, y_0, z_0) = (0, 0, 0)$:

$$\begin{cases} \dot{x} = z, \\ \dot{y} = -zg_1(x, y, z), \\ \dot{z} = g_2(x, y, z). \end{cases} \tag{1}$$

The system proposed and studied in this study adds the fourth equation of state and replaces $g_1(x, y, z)$ with $g_1(x, y, z, w) = ay + by^2 + xz - cw - d$ and $g_2(x, y, z)$ with $|x|^k + |y|^k - 1$. The system equation obtained is shown in thefollowing equation:

$$\begin{cases} \dot{x} = z, \\ \dot{y} = -z\left(ay + by^2 + xz - cw - d\right), \\ \dot{z} = |x|^k + |y|^k - 1, \\ \dot{w} = -ew - fyz. \end{cases} \tag{2}$$

Here, x, y, z, and w are state variables and a, b, c, d, e, f, and k are system parameters. Note that k is an integer. It is clear that the equilibrium points of the system are $\{(x, y, 0, 0): |x|^k + |y|^k = 1\}$. As shown in Figure 2, as k increases, the equation $||x|^k + |y|^k = 1$ forms a closed curve region with increasing k value.

System (2) can behave as chaos for $a = 5$, $b = 3$, $c = 32$, $d = 20$, $e = 0.01$, and $f = 25$; the initial conditions are assigned as $(x_0, y_0, z_0, w_0) = (0.02, 0.02, 0.02, 0.02)$. The Runge–Kutta method was used for numerical simulation, and simulation phase diagrams under different integers k were obtained, as shown in Figure 3. In Figures 3a–f of the simulation phase diagrams, the black closed curve is the equilibrium points under different integers k, and it can be seen that the attractor surrounds and connects the equilibria. It shows that the new system has a more complex phase diagram and satisfies at least one of the criteria [28].

According to System (2), the Jacobian matrix (3) of the system family can be obtained. The Lyapunov exponents were obtained by numerical simulation based on the famous Wolf's algorithm [29], as listed in Table 1.

$$J = \begin{bmatrix} 0 & 0 & 1 & 0 \\ -z^2 & -az - 2byz & -ay - by^2 - 2xz + cw + d & cz \\ kx^{k-1}[\mathrm{sgn}(x)]^k & ky^{k-1}[\mathrm{sgn}(y)]^k & 0 & 0 \\ 0 & -fz & -fy & -e \end{bmatrix}. \tag{3}$$

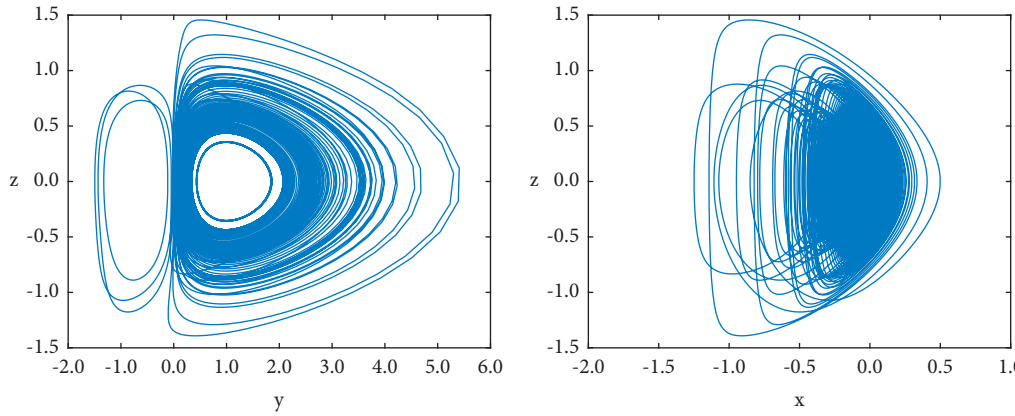

FIGURE 1: Chaotic phase diagram of System (1) with (a) = 5, (b) = 3, and $x(0) = [0\,0\,0]^T$ [9].

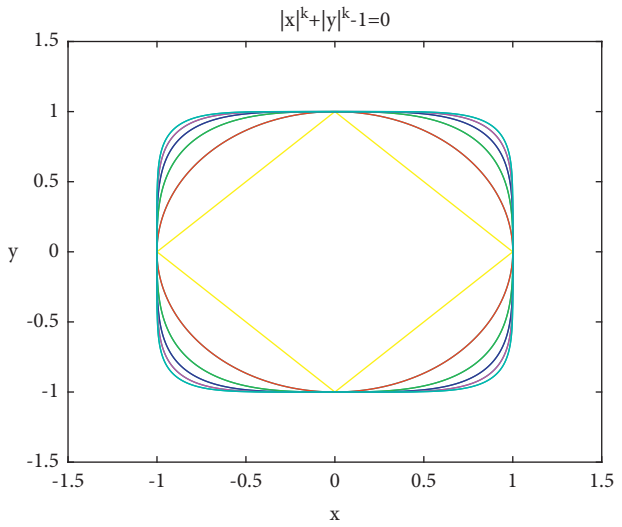

FIGURE 2: Set of equilibrium points of different shapes of the system when $k = 1, 2, 3, 4, 5, 6$.

3. Analysis of System Dynamics

We analyze the dynamics of the system at integer $k = 2$. For $a = 5$, $b = 3$, $c = 32$, $d = 20$, $e = 0.01$, and $f = 25$ and initial conditions $i_c = (0.02, 0.02, 0.02, 0.02)^T$, this system has chaotic solutions with the phase diagrams, as shown in Figure 4.

3.1. Equilibria Analysis and Lyapunov Exponents. When $k = 2$, the Jacobian matrix of the system at the equilibrium points [30] is illustrated in the following equation, where x^* and y^* are satisfied when $x^{*^2} + y^{*^2} = 1$:

$$J = \begin{bmatrix} 0 & 0 & 1 & 0 \\ 0 & 0 & -5y^* - 3y^{*2} + 20 & 0 \\ 2x^* & 2y^* & 0 & 0 \\ 0 & 0 & -fy^* & -e \end{bmatrix}. \quad (4)$$

Then, the characteristic polynomial of the Jacobian matrix is as follows:

$$\det(\lambda I - J) = 0. \quad (5)$$

The characteristic values at the equilibrium points obtained by numerical calculation are as follows:

$$\lambda_1 = -0.01, \quad \lambda_2 = 0, \lambda_{3,4} = \pm\sqrt{-6y^{*^3} - 10y^{*^2} + 40y^* + 2x^*}. \quad (6)$$

In Table 2, I, II, III, IV represent the four quadrants, respectively.

A pair of purely imaginary eigenvalues represents an unstable central equilibrium. And this implies an unstable saddle for pure real eigenvalues. In addition, the four-dimensional Bogdanov–Tarkens equilibrium ($\lambda_2 = \lambda_3 = \lambda_4 = 0$) for $k = 2$ is given.

This system has a chaotic solution with Lyapunov exponents $LE_1 = 0.0240$, $LE_2 = 0$, $LE_3 = -0.0172$, and $LE_4 = -0.0199$, and the Lyapunov exponential is shown in Figure 5.

The fractal dimension [17] can be calculated using the following equation:

$$D_L = j + \frac{1}{|LE_{j+1}|}\sum_{i=1}^{j} LE_i = 3 + \frac{LE_1 + LE_2 + LE_3}{|LE_4|} = 3.3417. \quad (7)$$

The Lyapunov exponents are $LE_1 > 0$, $LE_2 = 0$, $LE_3 < 0$, and $LE_4 < 0$, and the dimension is fractal ($D_L = 3.3417$). The system shows chaotic behavior.

3.2. Bifurcation Diagram and the Poincarè Section Diagram. Poincarè is a measure of the chaotic state that can effectively and directly describe the phase space [31]. The system is chaotic when the Poincarè map is a continuous curve or

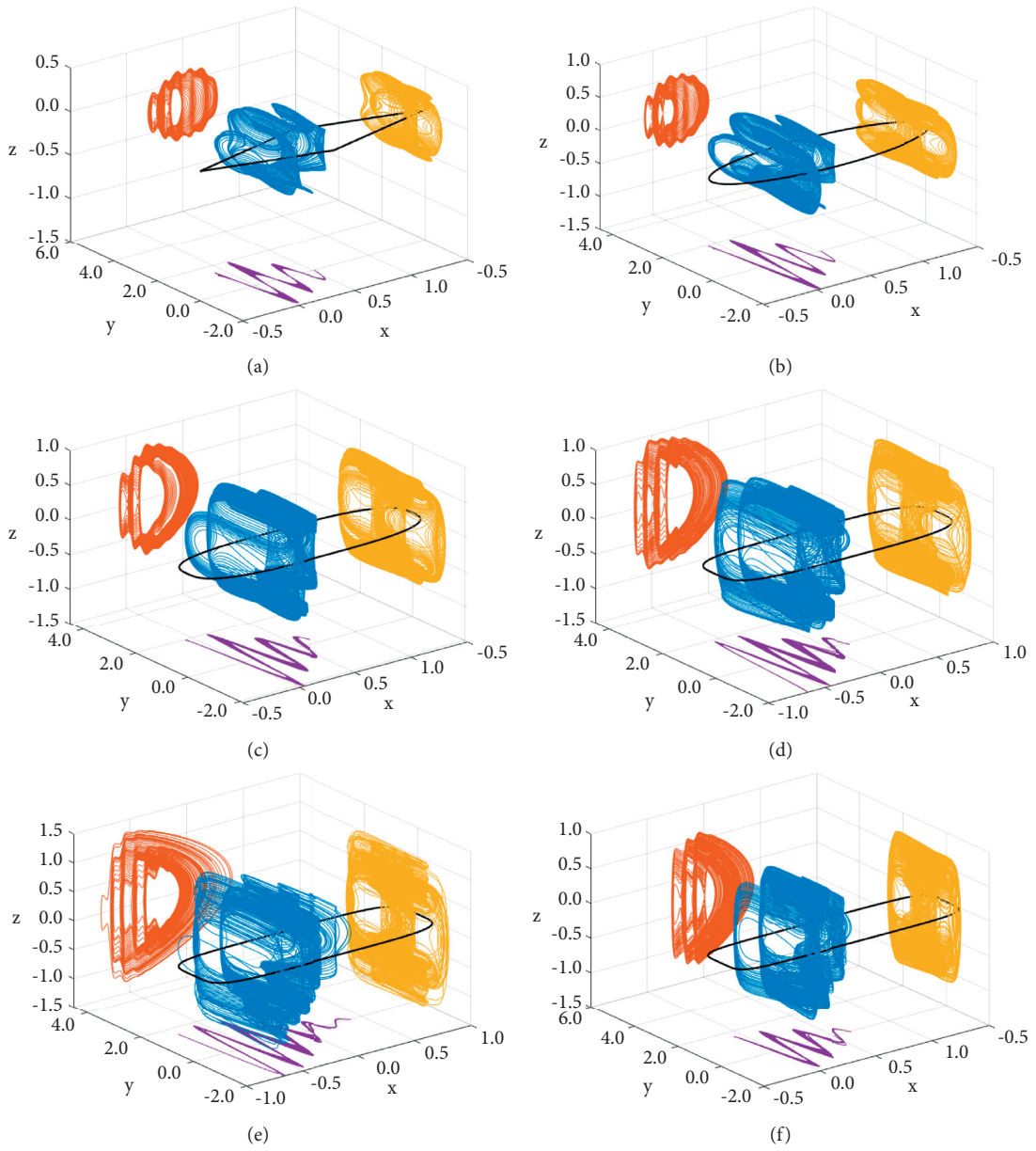

Figure 3: Phase diagram of the difference in integer k. (a) $k = 1$. (b) $k = 2$. (c) $k = 3$. (d) $k = 4$. (e) $k = 5$. (f) $k = 6$.

Table 1: Lyapunov exponents of different integers$k$.

Equations	Equilibria	LEs	D_{KY}
$k = 1$	$\lvert x^*\rvert + \lvert y^*\rvert = 1$	(0.0528, 0, −0.0200, −0.0400)	3.8200
$k = 2$	$(x^*)^2 + (y^*)^2 = 1$	(0.0240, 0, −0.0172, −0.0199)	3.3417
$k = 3$	$\lvert x^*\rvert^3 + \lvert y^*\rvert^3 = 1$	(0.0283 ,0, −0.0130, −0.0225)	3.6000
$k = 4$	$(x^*)^4 + (y^*)^4 = 1$	(0.0234 ,0, −0.0073, −0.0238)	3.6765
$k = 5$	$\lvert x^*\rvert^5 + \lvert y^*\rvert^5 = 1$	(0.0090, 0, −0.0047, −0.0125)	3.3440
$k = 6$	$(x^*)^6 + (y^*)^6 = 1$	(0.0144, 0, −0.0051, −0.0262)	3.3549

some dense points. The section diagram in Figure 6 shows an irregular distribution of points. Therefore, we can verify that the system is chaotic.

The bifurcation diagram can reflect the periodic or chaotic motion of a system [30]. If the parameters change, the stability of the system will vary. This is illustrated by

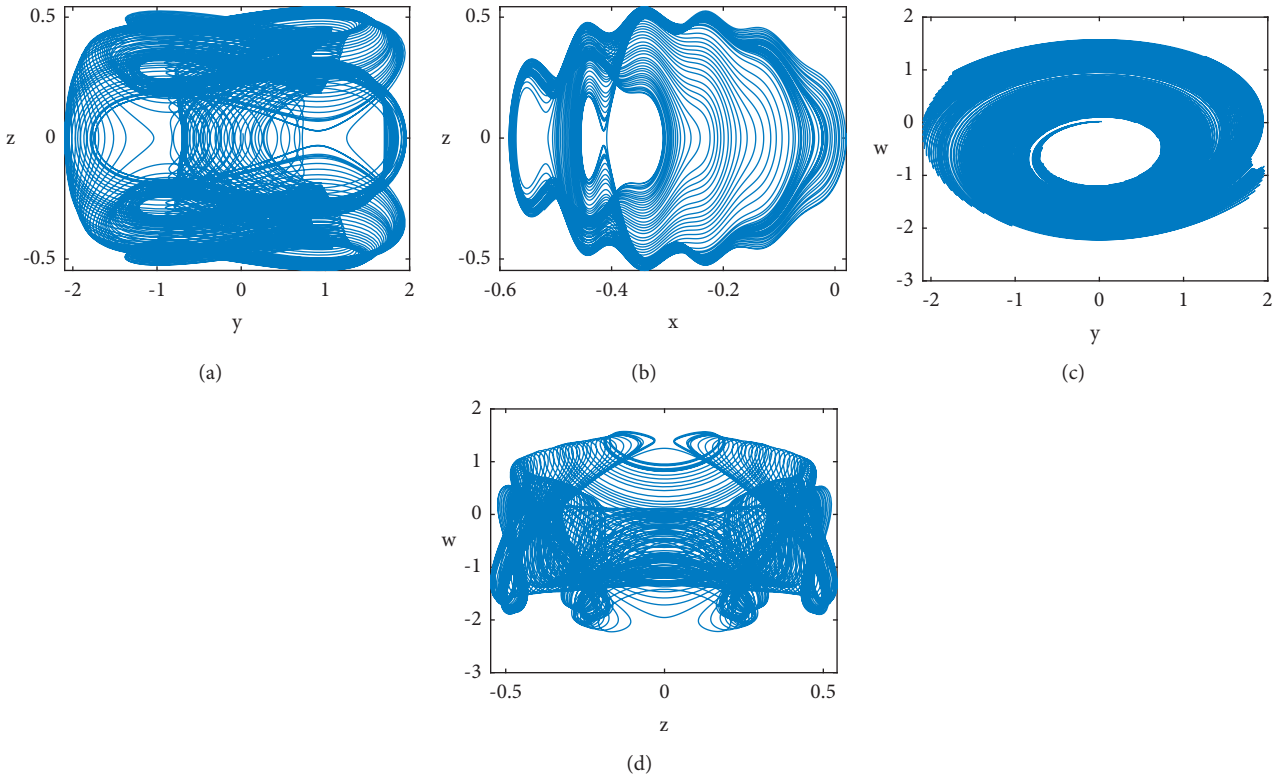

Figure 4: Chaotic system simulation two-dimensional phase diagram. (a) yz phase diagram. (b) xz phase diagram. (c) yw phase diagram. (d) zw phase diagram.

Table 2: Eigenvalues of system (2) for $k = 2$.

Case	$\lambda_{2,3}$
I	A pair of purely imaginary
II $-0.996 < x < 0,\ 0.05 < y < 1$	A pair of purely imaginary
II $-1 < x < -0.996,\ 0 < y < 0.05$	One positive real, one negative real
III	One positive real, one negative real
IV $0 < x < 0.996,\ -1 < y < -0.05$	One positive real, one negative real
IV $0.996 < x < 1,\ -0.05 < y < 0$	A pair of purely imaginary
$x = 0, y = 1$	$\lambda_{3,4} = \pm 4.8989$
$x = -1, y = 0$	$\lambda_{3,4} = \pm 1.4142i$
$x = 0, y = -1$	$\lambda_{3,4} = \pm 7.4833i$
$x = 1, y = 0$	$\lambda_{3,4} = \pm 1.4142$
$x = 0.996, y = -0.05$	$\lambda_{3,4} = 0$
$x = -0.996, y = 0.05$	$\lambda_{3,4} = 0$

observing the state changes of the chaotic system through the bifurcation diagram and Lyapunov exponential when the system parameter changes.

For $a = 5$, $b = 3$, $c = 32$, $d = 20$, $e = 0.01$, and $f \in [20, 100]$ this system has chaotic solutions with the bifurcation diagram and Lyapunov exponential, as shown in Figure 7. Obviously, from the bifurcation diagram and Lyapunov exponent spectrum, we conclude that System (2) exhibits robust chaos [32] in the whole region, except for the periodic motion shown when the maximum Lyapunov exponential zero at $f = 50$. Therefore, this type of system

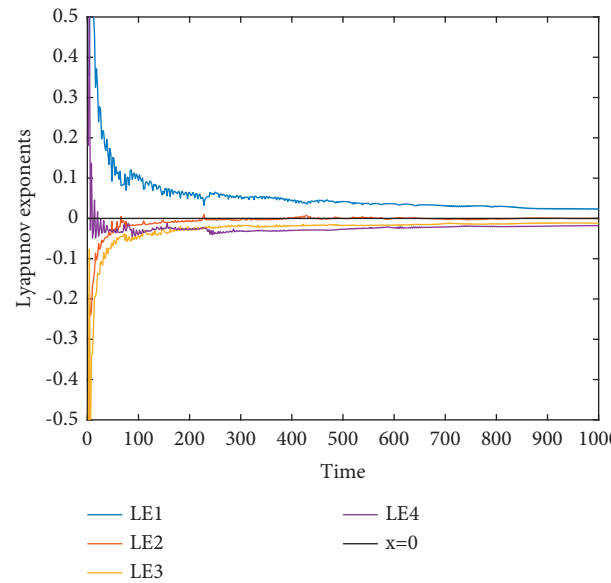

Figure 5: Lyapunov exponential of the system over time.

signal has high scientific research value and can be used in image encryption.

3.3. Multistability Analysis. Multiple stability is an interesting phenomenon, which usually exists in chaotic systems with infinite equilibrium points. It can be seen from the

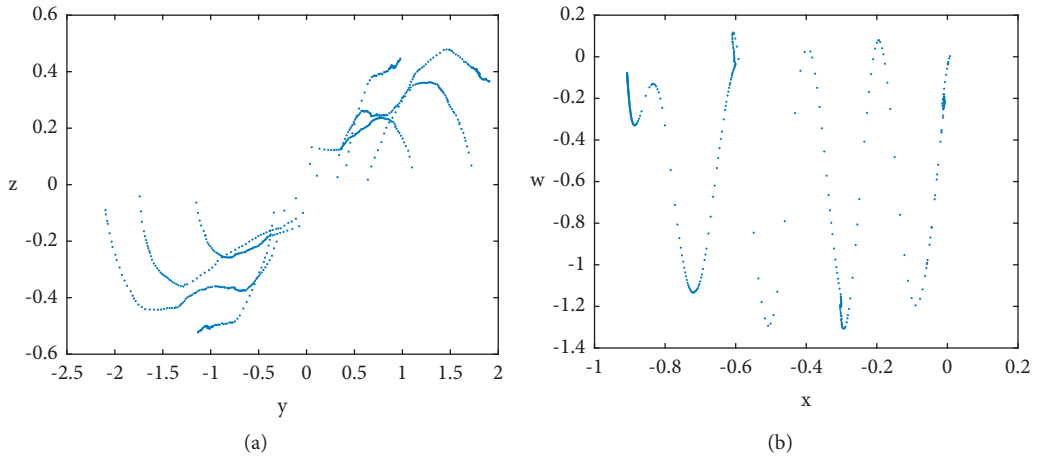

Figure 6: Poincarè diagram of the system. (a) Section $w = 0$ in the yzw phase diagram. (b) Section $z = 0$ in the xzw phase diagram.

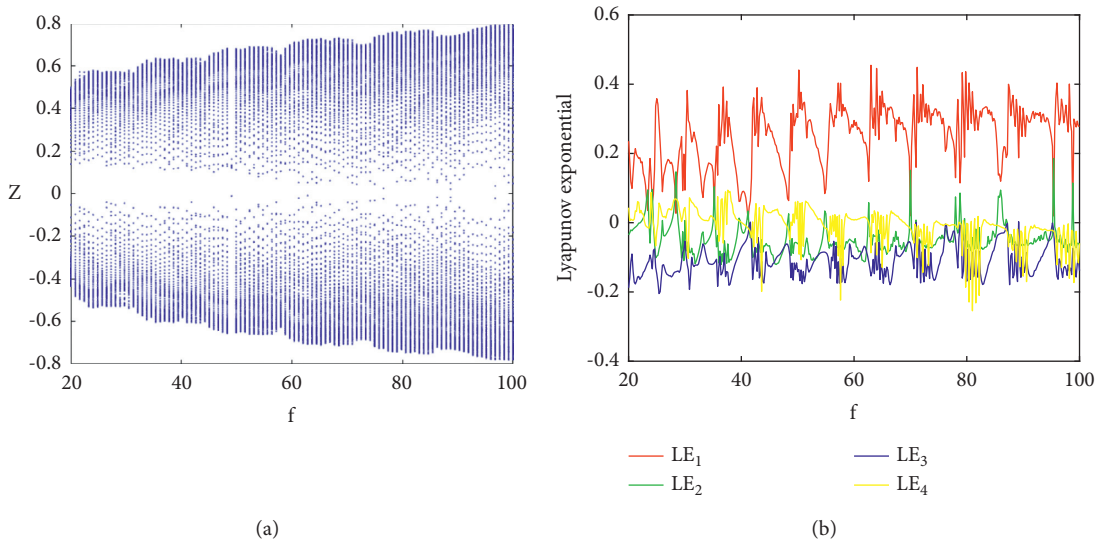

Figure 7: Bifurcation diagram and Lyapunov exponential spectrum of the system when parameter f changes. (a) Bifurcation diagram with f. (b) Lyapunov exponential with f.

bifurcation diagram in Figure 8. When the parameters $a = 5$, $b = 3, c = 32, d = 20, e = 0.01$, and varying f are in the region of [0, 30], there exist coexisting attractors. A set of initial conditions (0.02 0.02 0.02 0.02) with blue color and another set of initial conditions (0.5 0 0 0) with red color are fixed. Some sample coexisting attractors are presented. For example, when $f = 2.5$ or $f = 12.12$, the system produces the coexisting periodic attractors as shown in Figures 9(a) and 9(b). Moreover, the coexisting chaotic attractor and periodic attractor are found in the new System (2) with $f = 12.72$, as shown in Figure 9(c). In addition, the coexisting chaotic attractors are shown in Figure 9(d) with $f = 25$.

4. Implementation of System Circuit

Electronic circuit synthesis is not only a method to model nonlinear dynamic systems accurately but also a method to test the stability of system structures [11]. Multisim is used to design the circuit diagram of the chaotic system to illustrate

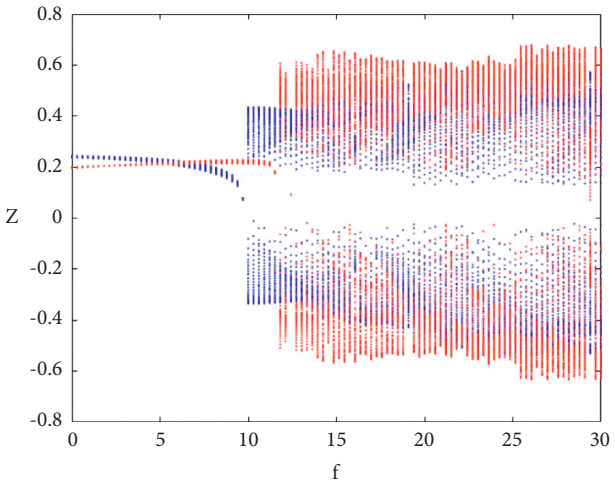

Figure 8: Coexisting bifurcation diagram of the state variable z with respect to the control parameter f.

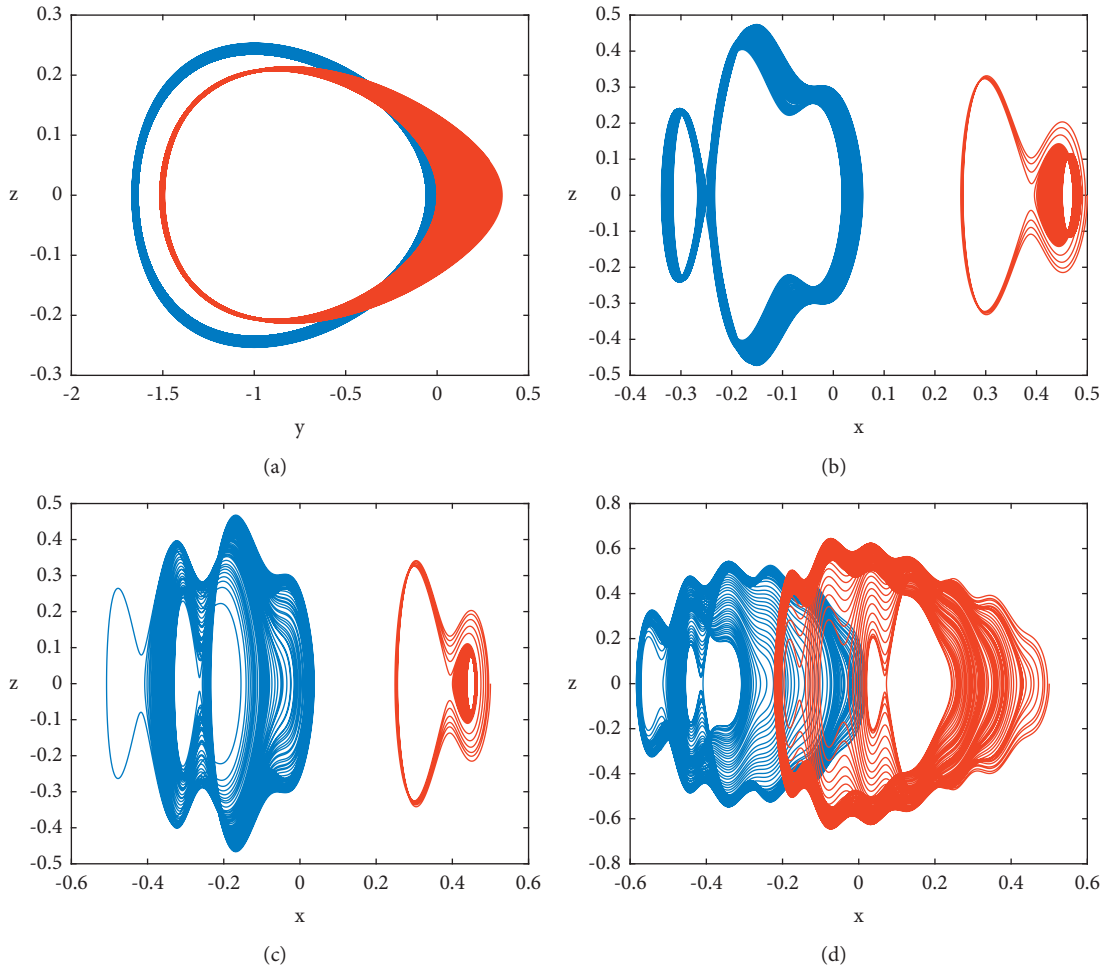

Figure 9: (a) The coexisting periodic attractors in y-z plane. (b) The coexisting periodic attractors in x-z plane. (c) The coexisting chaotic attractor and periodic attractor in x-z plane. (d) The coexisting chaotic attractors in x-z plane.

the feasibility of the system, as shown in Figure 10. We use the popular design approach based on multipliers and operational amplifiers, which is TL082CD, the supply voltage is ±15V, and the saturation voltage is ±13.5V. The multiplier is AD633 (the output gain is set to 0.1).

Under the classical system parameters, the dynamic range of the state variable of System (2) is too small. In order to avoid excessive input errors of the multiplier, the linear transformation of the state variable of the system of equation (8) is performed and then the time scale transformation [33] of $\tau = \tau_0 t$ is performed. Finally, the system of equation (9) is obtained.

A schematic diagram of the designed circuit is shown in Figure 9. When the capacitance values are $C_1 = C_2 = C_3 = C_4 = 0.1\mu F$ and the resistor values are $R_{12} = R_{13} = R_{14} = R_{15} = R_{16} = R_{17} = 10k\Omega$, the other resistor values are shown in equation (10):

$$(x, y, z, w) \longrightarrow (0.1x, 0.25y, 0.05z, 0.25w), \tag{8}$$

$$\begin{cases} \dot{x} = 500z, \\ \dot{y} = -250zy - 37.5y^2z - xz^2 - 1600w(-z) - 4000(-z), \\ \dot{z} = -200x^2 + 1250y^2 - 20000, \\ \dot{w} = -10w - 1250yz. \end{cases} \tag{9}$$

The phase diagram obtained by circuit simulation is shown in Figure 11. Comparing the circuit simulation phase

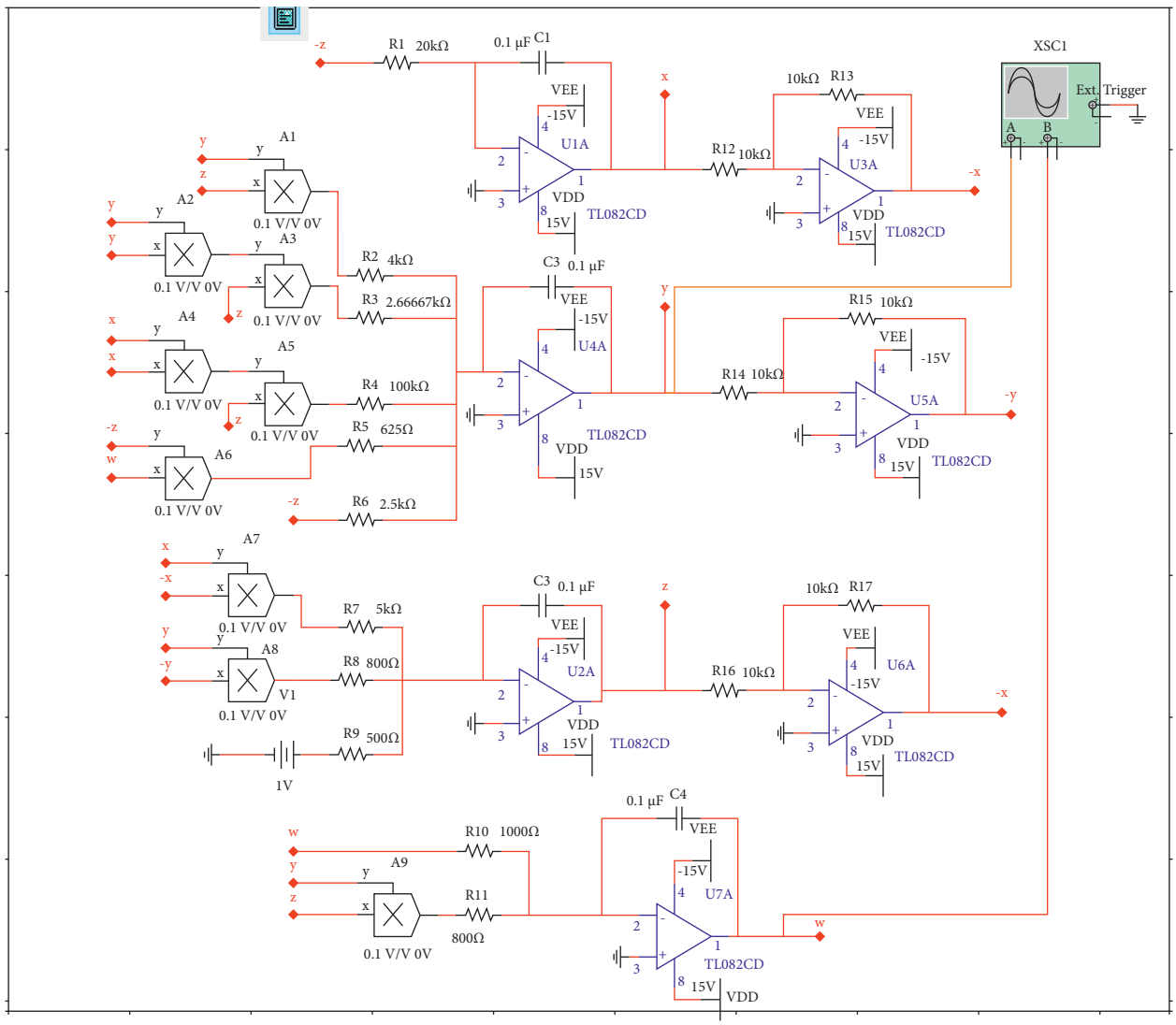

Figure 10: Circuit diagram of the chaotic system.

diagrams in Figure 11 and the numerical simulation phase diagrams in Figure 4 shows that they coincide, which verifies the circuit feasibility of the chaotic system.

$$
\begin{cases}
500 = \dfrac{1}{R_1 C_1} \longrightarrow R_1 = 20\,k\Omega, 250 = \dfrac{1}{R_2 C_2} \longrightarrow R_2 = 4\,k\Omega, \\
37.5 = \dfrac{1}{R_3 C_2} \longrightarrow R_3 = 2.6\,k\Omega, 1 = \dfrac{1}{R_4 C_2} \longrightarrow R_4 = 100\,k\Omega, \\
1600 = \dfrac{1}{R_5 C_2} \longrightarrow R_5 = 625\,\Omega, 4000 = \dfrac{1}{R_6 C_2} \longrightarrow R_6 = 2.5\,k\Omega, \\
200 = \dfrac{1}{R_7 C_3} \longrightarrow R_7 = 5k\,\Omega, 1250 = \dfrac{1}{R_8 C_3} \longrightarrow R_8 = 800\,\Omega, \\
20000 = \dfrac{1}{R_9 C_3} \longrightarrow R_9 = 500\,\Omega, 10 = \dfrac{1}{R_{10} C_4} \longrightarrow R_{10} = 1000\,k\Omega, \\
1250 = \dfrac{1}{R_{11} C_4} \longrightarrow R_{11} = 800\,\Omega.
\end{cases}
\tag{10}
$$

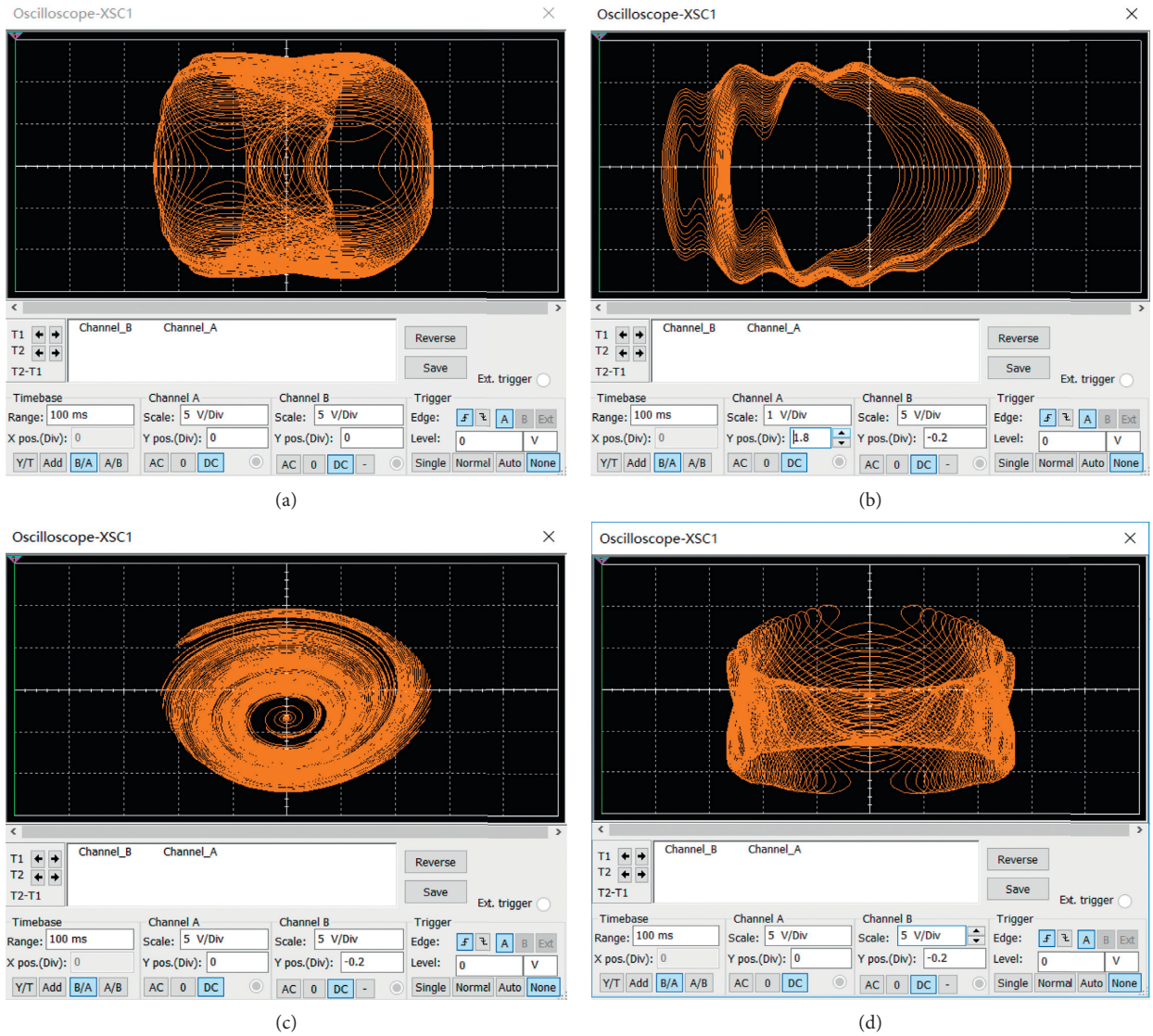

FIGURE 11: Circuit simulation phase diagram. (a) yz phase diagram. (b) xz phase diagram. (c) yw phase diagram. (d) zw phase diagram.

5. Parameter Adaptive Synchronous Control

In this study, the synchronous control of two systems with infinite equilibrium points is studied.

The drive system with an infinite equilibrium point is designed as follows:

$$\begin{cases} \dot{x_1} = x_3, \\ \dot{x_2} = -ax_2x_3 - b{x_2}^2x_3 - x_1{x_3}^2 + cx_3x_4 + \mathrm{d}x_3, \\ \dot{x_3} = {x_1}^2 + {x_2}^2 - 1, \\ \dot{x_4} = -ex_4 - fx_2x_3. \end{cases} \tag{11}$$

The designed response system is as follows:

$$\begin{cases} \dot{y}_1 = y_3 + u_1, \\ \dot{y}_2 = -\hat{a}y_2y_3 - \hat{b}{y_2}^2y_3 - y_1{y_3}^2 + \hat{c}y_3y_4 + \hat{d}y_3 + u_2, \\ \dot{y}_3 = {y_1}^2 + {y_2}^2 - 1 + u_3, \\ \dot{y}_4 = -\hat{e}y_4 - \hat{f}y_2y_3 + u_4. \end{cases} \tag{12}$$

Here, the adaptive controller is $u = [u_1, u_2, u_3, u_4]^T$ and the state error of the drive system and the response system is defined as $e_i = y_i - x_i (i = 1, 2, 3, 4)$. The synchronization state error is calculated by the following equation [34]:

$$\begin{cases} e_1 = y_1 - x_1, \\ e_2 = y_2 - x_2, \\ e_3 = y_3 - x_3, \\ e_4 = y_4 - x_4. \end{cases} \tag{13}$$

Similarly, the estimated error of the calculated parameters is as follows:

$$\begin{cases} e_a = a - \hat{a}, \\ e_b = b - \hat{b}, \\ e_c = c - \hat{c}, \\ e_d = d - \hat{d}, \\ e_e = e - \hat{e}, \\ e_f = f - \hat{f}, \end{cases} \tag{14}$$

$$\begin{cases} \dot{e}_a = -\dot{\hat{a}}, \\ \dot{e}_b = -\dot{\hat{b}}, \\ \dot{e}_c = -\dot{\hat{c}}, \\ \dot{e}_d = -\dot{\hat{d}}, \\ \dot{e}_e = -\dot{\hat{e}}, \\ \dot{e}_f = -\dot{\hat{f}}, \end{cases} \tag{15}$$

where $\hat{a}, \hat{b}, \hat{c}, \hat{d}, \hat{e}$, and $\hat{f}$ are the estimated of parameters. The estimation error of the dynamic parameters can be obtained by equation (15).

To achieve adaptive synchronous control, namely, to achieve $\lim_{t\longrightarrow+\infty}\|e(t)\| = \lim_{t\longrightarrow+\infty}\|y(t) - x(t)\| = 0$, the adaptive controller is designed as follows:

$$\begin{cases} u_1 = -e_3 - k_1e_1, \\ u_2 = \hat{a}(e_2e_3 + e_2x_3 + e_3x_2) + \hat{b}\left({y_2}^2y_3 - {x_2}^2x_3\right) + y_1{y_3}^2 - x_1{x_3}^2 - \hat{c}(e_3e_4 + e_3x_4 + e_4x_3) - \hat{d}e_3 - k_2e_2, \\ u_3 = -e_1(y_1 + x_1) - e_2(y_2 + x_2) - k_3e_3, \\ u_4 = \hat{e}e_4 + \hat{f}(e_2e_3 + e_2x_3 + e_3x_2) - k_4e_4. \end{cases} \tag{16}$$

Here, k_1, k_2, k_3, and k_4 are normal numbers, and the parameter updating law is defined as follows:

$$\begin{cases} \dot{\hat{a}} = -\lambda_1\left(e_2^2e_3 + e_2^2x_3 + e_2e_3x_2 - e_a\right), \\ \dot{\hat{b}} = -\lambda_2\left(e_2{y_2}^2y_3 - e_2{x_2}^2x_3\right) - e_b, \\ \dot{\hat{c}} = \lambda_3(e_2e_3e_4 + e_2e_3x_4 + e_2e_4x_3 + e_c), \\ \dot{\hat{d}} = \lambda_4(e_2e_3 + e_d), \\ \dot{\hat{e}} = -\lambda_5\left(e_4^2 - e_e\right), \\ \dot{\hat{f}} = -\lambda_6\left(e_2e_3e_4 + e_2e_4x_3 + e_3e_4x_2 - e_f\right). \end{cases} \tag{17}$$

The designed controller and parameter updating rules are inserted into the error equation to obtain the following equation:

$$\begin{cases} \dot{e}_1 = -k_1e_1, \\ \dot{e}_2 = -e_a(e_2e_3 + e_2x_3 + e_3x_2) - e_b\left({y_2}^2y_3 - {x_2}^2x_3\right) + e_c(e_3e_4 + e_3x_4 + e_4x_3) + e_de_3 - k_2e_2, \\ \dot{e}_3 = -k_3e_3, \\ \dot{e}_4 = -e_ee_4 - e_f(e_2e_3 + e_2x_3 + e_3x_2) - k_4e_4. \end{cases} \tag{18}$$

Lyapunov stability theory [16, 35] was used to verify the synchronization of the drive system and response system. The Lyapunov function is constructed as follows:

$$V\left(e_1, e_2, e_3, e_4, e_a, e_b, e_c, e_e, e_f\right) = \frac{1}{2}e_1^2 + \frac{1}{2}e_2^2 + \frac{1}{2}e_3^2 + \frac{1}{2}e_4^2 + \frac{1}{2\lambda_1}e_a^2 + \frac{1}{2\lambda_2}e_b^2 + \frac{1}{2\lambda_3}e_c^2\frac{1}{2\lambda_4}e_d^2 + \frac{1}{2\lambda_5}e_e^2 + \frac{1}{2\lambda_6}e_f^2. \tag{19}$$

In equations (17) and (19), factor $\lambda_i > 0\,(i = 1, 2, 3, 4, 5, 6)$ and the derivative of V yields equation (20), which is obvious for $V \geq 0$ and $\dot{V} < 0$. Therefore, according to Lyapunov stability theory, the driving system and the response system can realize synchronization.

The synchronization is verified by an example. That is, the fourth-order Runge–Kutta algorithm is used for numerical simulation. The system parameters are $a = 5$, $b = 3$, $c = 32$, $d = 20$, $e = 0.01$, and $f = 25$. The initial values of the drive system are $x_1(0) = 0.01$, $x_2(0) = 0.01$, $x_3(0) = 0.01$, and $x_4(0) = 0.01$. The initial values of the response system are $y_1(0) = 2$, $y_2(0) = 4$, $y_3(0) = 6$, and $y_4(0) = 8$. The initial conditions of the parameter estimation are $\widehat{a} = 2.5$, $\widehat{b} = 1.5$, $\widehat{c} = 35$, $\widehat{d} = 25$, $\widehat{e} = 0.02$, and $\widehat{f} = 20$. The control parameters are set as $k_1 = k_2 = k_3 = k_4 = 80$ and $\lambda_1 = \lambda_2 = \lambda_3 = \lambda_4 = \lambda_5 = \lambda_6 = 60$. The simulation results are shown in Figure 12.

$$\begin{aligned}
\dot{V} = {} & e_1\dot{e}_1 + e_2\dot{e}_2 + e_3\dot{e}_3 + e_4\dot{e}_4 + \frac{1}{\lambda_1}e_a\dot{e}_a + \frac{1}{\lambda_2}e_b\dot{e}_b + \frac{1}{\lambda_3}e_c\dot{e}_c + \frac{1}{\lambda_4}e_d\dot{e}_d + \frac{1}{\lambda_5}e_e\dot{e}_e + \frac{1}{\lambda_6}e_f\dot{e}_f = -k_1e_1^2 \\
& - e_ae_2\left(e_2e_3 + e_2x_3 + e_3x_2\right) \\
& - e_be_2\left({y_2}^2y_3 - {x_2}^2x_3\right) + e_ce_2\left(e_3e_4 + e_3x_4 + e_4x_3\right) \\
& + e_de_2e_3 - k_2e_2^2 - k_3e_3^2 - e_ee_4^2 - e_fe_4\left(e_2e_3 + e_2x_3 + e_3x_2\right) - k_4e_4^2 \\
& - \frac{1}{\lambda_1}e_a\dot{\widehat{a}} - \frac{1}{\lambda_2}e_b\dot{\widehat{b}} - \frac{1}{\lambda_3}e_c\dot{\widehat{c}} - \frac{1}{\lambda_4}e_d\dot{\widehat{d}} - \frac{1}{\lambda_5}e_e\dot{\widehat{e}} - \frac{1}{\lambda_6}e_f\dot{\widehat{f}}\,, \\
= {} & -k_1e_1^2 + e_a\left(-e_2\left(e_2e_3 + e_2x_3 + e_3x_2\right) - \frac{1}{\lambda_1}\dot{\widehat{a}}\right) + e_b\left(-e_2\left({y_2}^2y_3 - {x_2}^2x_3\right) - \frac{1}{\lambda_2}\dot{\widehat{b}}\right) \\
& + e_c\left(e_2\left(e_3e_4 + e_3x_4 + e_4x_3\right) - \frac{1}{\lambda_3}\dot{\widehat{c}}\right) - k_2e_2^2 - k_3e_3^2 + e_d\left(e_2e_3 - \frac{1}{\lambda_4}\dot{\widehat{d}}\right) \\
& + e_e\left(-e_4^2 - \frac{1}{\lambda_5}\dot{\widehat{e}}\right) + e_f\left(-e_4\left(e_2e_3 + e_2x_3 + e_3x_2\right) - \frac{1}{\lambda_6}\dot{\widehat{f}}\right) - k_4e_4^2 \\
= {} & -e_a^2 - e_b^2 - e_c^2 - e_d^2 - e_e^2 - e_f^2 - k_1e_1^2 - k_2e_2^2 - k_3e_3^2 - k_4e_4^2.
\end{aligned} \tag{20}$$

The synchronization error curves between the driving system and the response system are achieved in approximately 0.08 seconds. The system completes the identification of unknown parameters in approximately 0.1 seconds. This shows that the synchronization control of the two systems is realized and that the synchronization effect is good. But in different synchronization systems, the control parameters are selected differently, reflecting different synchronization effects. Therefore, the choice of control parameters should depend on the specific situation.

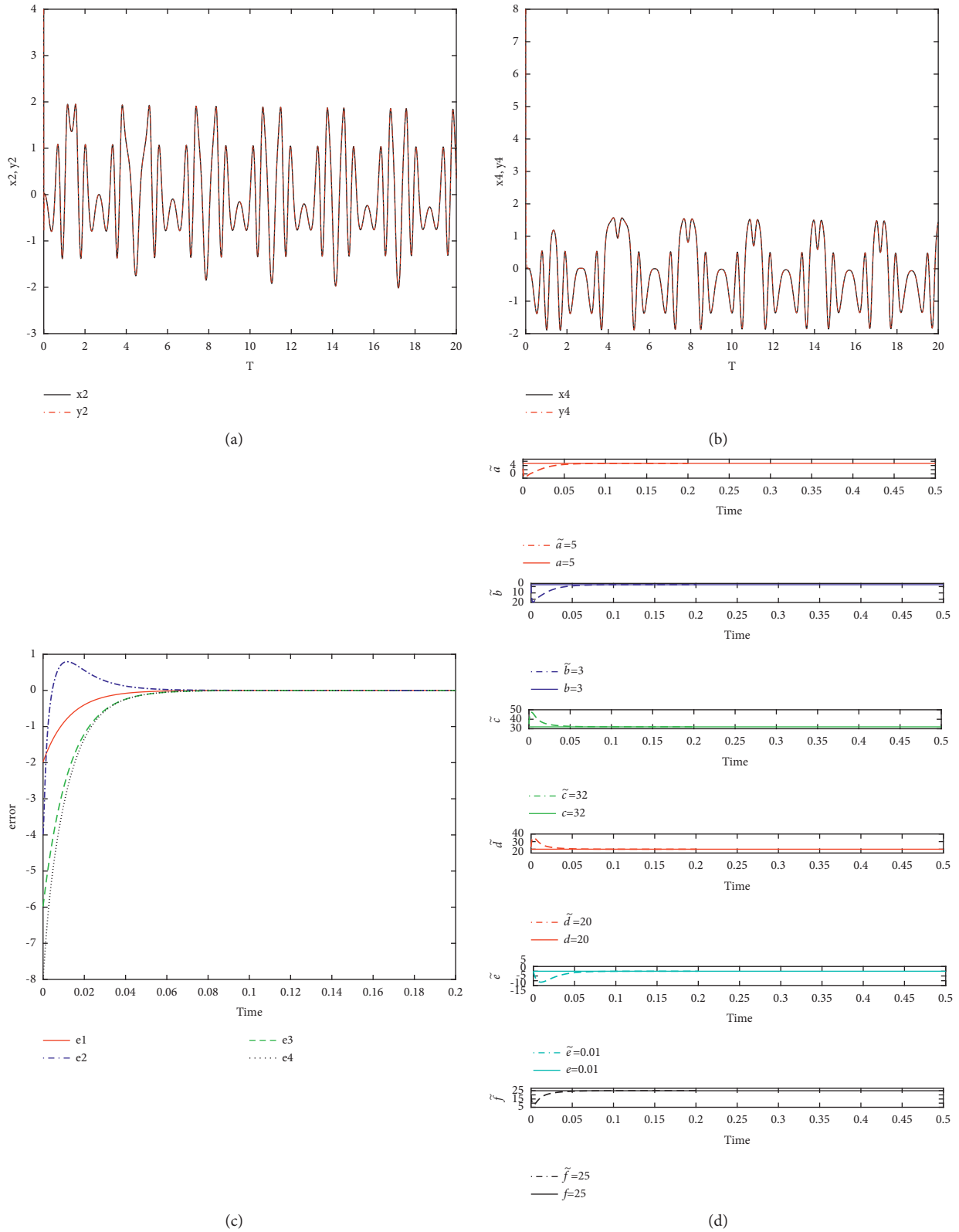

Figure 12: Synchronous simulation. (a) Synchronization waveform of x_2 and y_2. (b) Synchronization waveform of x_4 and y_4. (c) Synchronization errors e_1, e_2, e_3, and e_4. (d) Identification curves of parameters.

6. Application in Image Encryption

In cryptography, there are some basic concepts [36], such as plaintext representing information to be encrypted, ciphertext representing information processed by an encryption algorithm, an encryption algorithm representing the way plaintext converted to ciphertext, and a decryption algorithm representing the way ciphertext converted to plaintext. There are two principles for encryption in cryptography: diffusion and confusion. Diffusion is the purpose of encrypting plaintext by loading plaintext into ciphertext [16]. However, confusion uses obfuscation to conceal the relationship between plaintext and ciphertext without changing the plaintext, making the plaintext undecipherable. The analysis of the image encryption effect mainly includes histograms, information entropy, sensitivities to keys, correlations, and other measures. The overall structure of the image encryption and decryption process of this study is shown in Figure 13.

6.1. Method of Image Encryption and Decryption Method. In this study, a chaotic adaptive parameter synchronization control system with infinite equilibria is used for image encryption to verify that the system is more secure for cryptography.

There are 3-color data matrices R, G, and B of original image I with $512 \times 512 \times 3$ pixels. The original image I is denoted as $M \times N$.

The detailed steps of image encryption are as follows:

Step 1: Preprocess the chaotic sequences.

When the initial values of the adaptive parameter system are $x_1(0) = 0.01$, $x_2(0) = 0.02$, $x_3(0) = 0.01$, and $x_4(0) = 0.02$, the four-dimensional chaotic sequences of the driving system, which are denoted as $x = [x_1, x_2, x_3, x_4]^T$, can be obtained. To eliminate the transient effects for more random effects, the top 1000 items generated iteratively were removed. Each element ($c(i)$) in the chaotic sequences was processed by the following equation, and the chaotic sequences were converted into an integer between 0 and 255:

$$c(i) = \left(\left(c(i) * 10^3\right) \bmod 256\right). \tag{21}$$

Step 2: Generate scrambled sequences. Three chaotic sequences of x_1, x_2, and x_3 were arranged in ascending order with the sort function to obtain the scrambled matrices R', G', and B'.

Step 3: The chaotic sequence x4 obtained by iteration is transformed into a two-dimensional matrix C, whose size is $M \times N$. The XOR operation [16] (Table 3) was performed on matrices R', G', and B', and matrix C is obtained according to number 1 in Table 4 (binary code for DNA coding rules [16]) at corresponding positions to conceal plaintext information. The diffusion matrices R'', G'', and B'' are obtained.

Step 4: Reconstruct the matrices R'', G'', and B'' to obtain the encrypted image.

The detailed steps of the image decryption are as follows:

Step 1. Preprocessed sequences. Input the initial values of the adaptive parameters system as the keys to obtain the 4-dimensional mixture of the response system. It is denoted as $y = [y_1, y_2, y_3, y_4]^T$. Similarly, the first 1000 items are eliminated, and then each element in the chaotic sequences is processed by equation (21) to convert the chaotic sequences into an integer between 0 and 255.

Step 2. Read the 3-color ciphertext matrices R'', G'', and B'' of the encrypted image.

Step 3. The resulting chaotic sequence y_4 is converted to a two-dimensional matrix C' with a size of $M \times N$. The XOR operation (Table 3) is performed on the ciphertext matrices R'', G'', and B'', and matrix C' at the corresponding positions according to number 1 in Table 4 (binary rules for DNA encoding [14]). The R', G', and B' matrices of the ciphertext image are obtained.

Step 4. The R', G', and B' matrices of the ciphertext image are restored by using x_1, x_2, and x_3 chaotic sequences as ascending obfuscations. The R, G, and B matrices are obtained.

Step 5. Reconstruct two-dimensional matrices R, G, and B. The decrypted image is obtained.

6.2. Experimental Simulation. In this study, the classic image Lena is used as the representative for encryption. The adaptive parameter system selects the above parameters and conducts encryption according to the above steps.

Figure 14 shows the experimental results. It can be seen that the encrypted image has no similar information to the original image, and it can be visually determined that the encryption and decryption are successful.

6.3. Histogram Analysis. The histogram intuitively sees the encryption effect. Figure 15 is a histogram comparison of original and encrypted images in the RGB channels.

Figure 15 shows that the histograms of the encrypted image are completely different from those of the original image. The pixel values of ciphertext images are evenly distributed by diffusion, and it is difficult to analyze the relationship with the original image. The hiding effect of the pixel values of the original image is better.

6.4. Correlation Analysis. The adjacent pixels of the original image have large correlations in the horizontal, vertical, and diagonal directions because of the coherence of the picture. Image encryption destroys the correlation between the pixel values of the original image. Therefore, correlation analysis can be used as an index of image encryption effect analysis. N pairs of adjacent pixels, which are (u_i, v_i), from the image are chosen. The correlation coefficient [37] is calculated by equation (22). The correlation curves are shown in Figure 16, and the correlation coefficients are listed in Table 5.

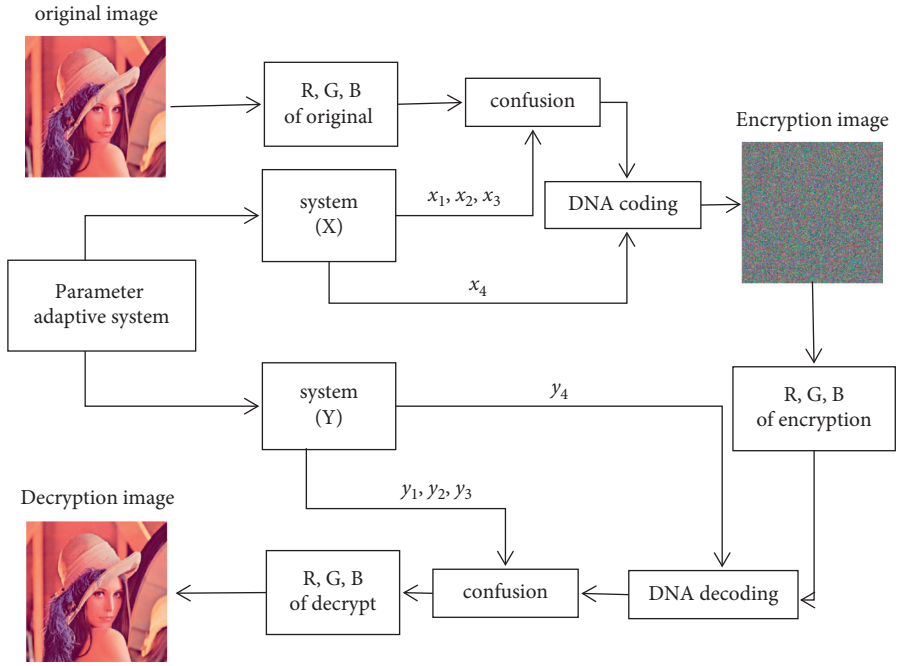

Figure 13: The overall structure of the image encryption and decryption.

Table 3: Xor operation.

⊕	A	T	C	G
A	T	A	G	C
T	A	T	C	G
C	G	C	T	A
G	C	G	A	T

Table 4: Binary versus DNA coding rules.

	0	1	2	3	4	5	6	7
A	00	00	11	11	01	01	10	10
T	11	11	00	00	10	10	01	01
C	10	01	10	01	11	00	11	00
G	01	11	01	11	00	11	00	11

$$\begin{cases} r_{xy} = \dfrac{\operatorname{cov}(u,v)}{\sqrt{D(u)}\sqrt{D(v)}}, \\ \operatorname{cov}(u,v) = \dfrac{1}{N}\displaystyle\sum_{i-1}^{N}\left(u_i - E(u)\right)\left(y_i - E(v)\right), \\ D(u) = \dfrac{1}{N}\displaystyle\sum_{i-1}^{N}\left(u_i - E(u)\right)^2, \\ E(u) = \dfrac{1}{N}\displaystyle\sum_{i-1}^{N} u_i. \end{cases} \tag{22}$$

The correlations of the original image and the ciphered image show that the pixel correlation can be reduced to zero or close to zero after encryption. After encrypting adjacent pixels, it is concluded that the algorithm has a secure encryption effect. This means that the attacker cannot use correlation to crack the encrypted image.

6.5. Information Entropy Analysis. Information entropy reflects the uncertainty of image information [26] and can be calculated by the following equation [37]:

$$H = -\sum_{i=0}^{L} p(i)\log_2 p(i), \tag{23}$$

where L is the number of gray levels of the image and $p(i)$ is the probability of the pixel value in the entire picture. The theoretical value of the information entropy is 8. It is generally believed that the information entropy of all the encrypted images is quite close to the ideal value of 8, which implies that the encrypted images have good randomness.

As Table 6 shows, the encryption algorithm performs better than the results in the listed literature, which indicates that this encryption algorithm is competitive in this sense.

6.6. Key Sensitivity Analysis. Key sensitivity [38] means that a small change in a designed key will lead to decryption failure, and the original image cannot be extracted when the same image is decrypted.

The keys used in this study that decrypt the image are the $y_1(0) = 0.01$, $y_2(0) = 0.02$, $y_3(0) = 0.01$, and $y_4(0) = 0.02$, as shown in Figure 17(a). $y(0) = y(0) + 10^{-16}$ is slightly changed and the other keys remained unchanged. The decrypted image is shown in Figure 17.

Figure 17(a) shows that the decryption image is completely identical to the original image. However, in

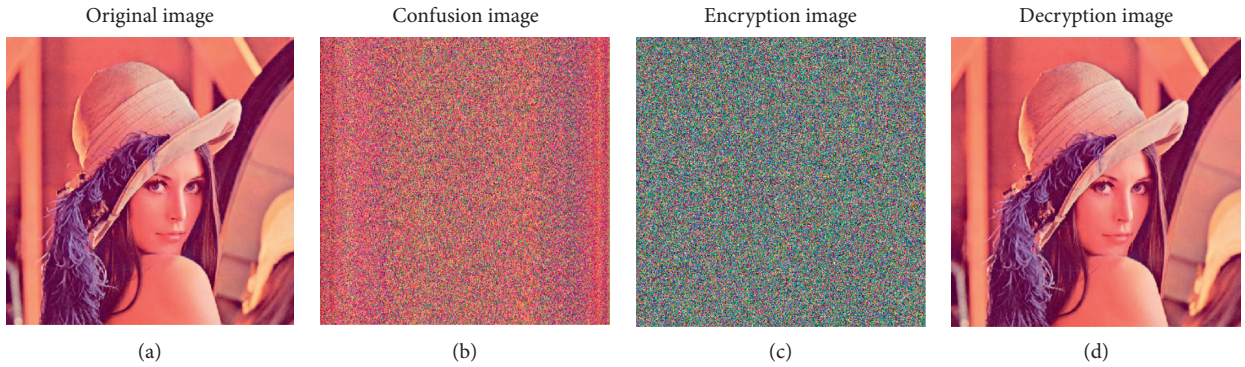

Figure 14: Encryption results. (a) Original image. (b) Confusion image. (c) Encryption image. (d) Decryption image.

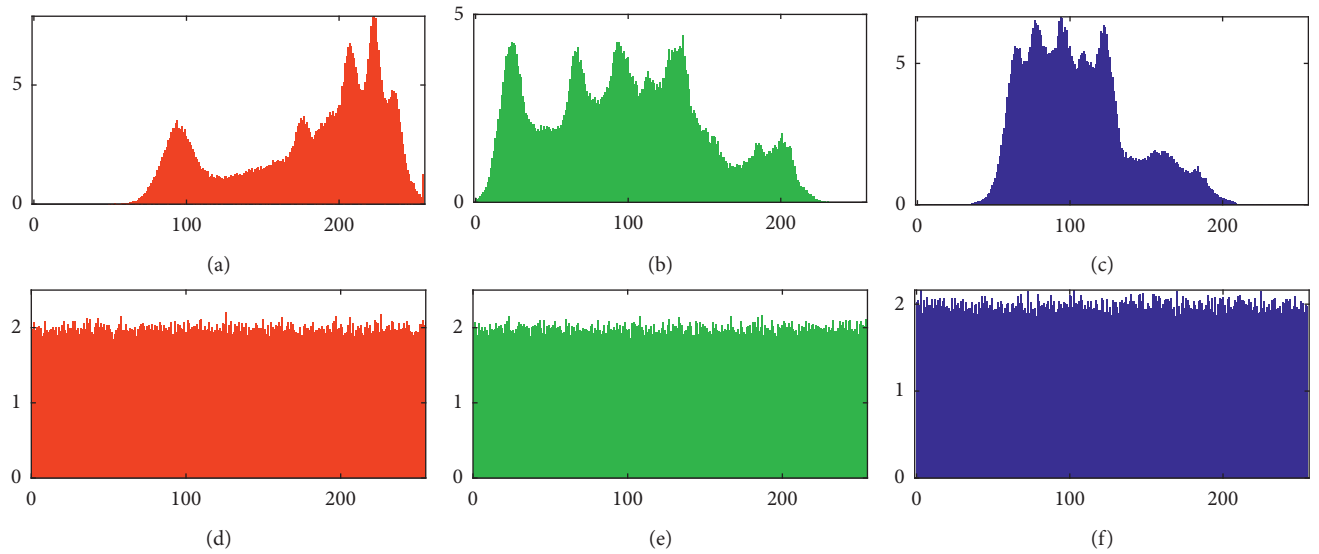

Figure 15: Histograms analysis. (a–c) Histograms of the original image in the RGB channels, respectively; (d–f) histograms of the encrypted image in RGB channels, respectively.

Figure 17(b), the decryption image is completely different, which means that the proposed encryption method provides a high decrypt sensitivity.

7. Discussions

The proposed family of chaotic systems enriches the study of chaotic systems with infinite equilibrium points, and on this basis, we can independently study chaotic systems with more unique closed curve equilibrium points. The integer-order chaotic system can also be extended to the fractional-order chaotic system, so that the study of chaotic system has more practical significance. The circuit of the new system is designed and simulated with Multisim. The phase diagram of the circuit simulation is in good agreement with the result of numerical simulation. This proves the feasibility of circuit realization, and chaotic systems can be realized by analog and digital circuit construction in the future work, which endods the value of the industrial practical application of the chaotic system. The designed adaptive synchronization control can achieve synchronization quickly. However, other synchronization control technologies can be expanded to achieve faster synchronization for a better synchronization effect. The combination of synchronous control and DNA encoding in image encryption can effectively improve the security performance of encryption/decryption, which has further research value. Furthermore, extending the synchronization control of chaotic system to the application

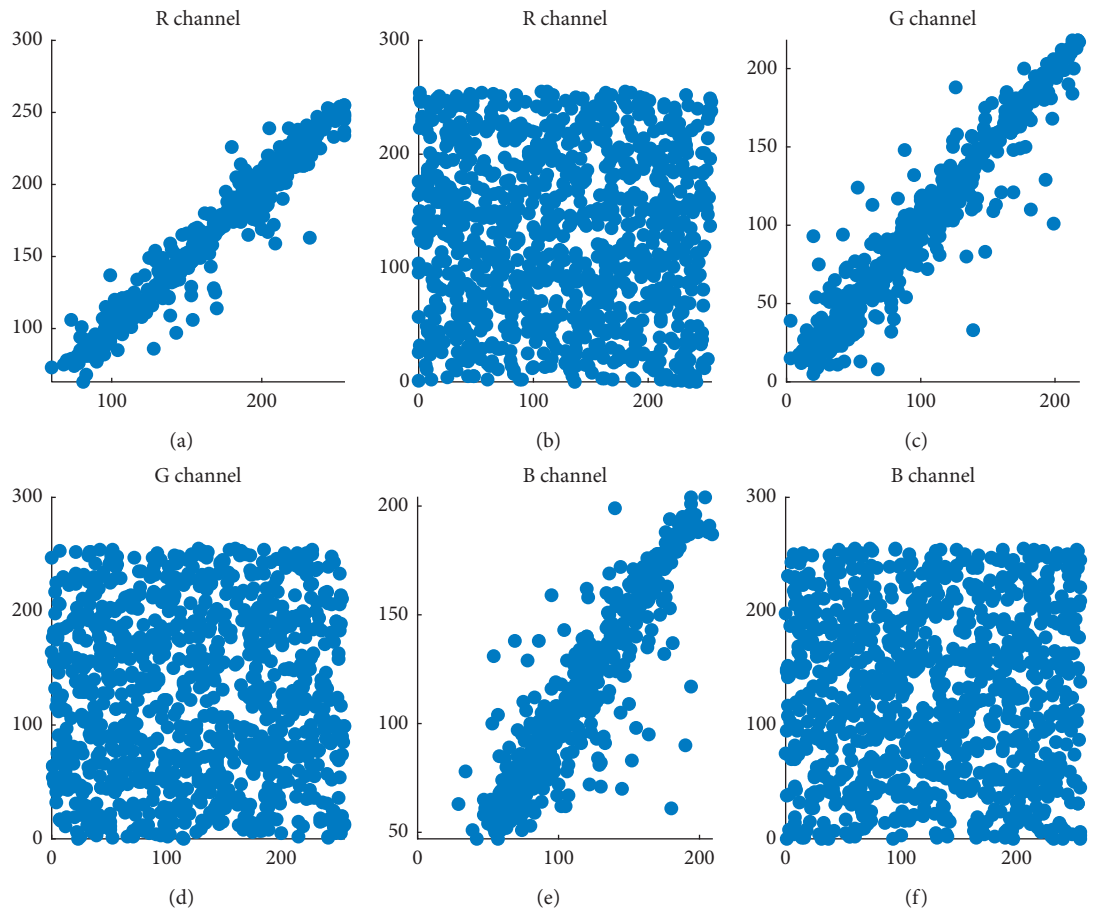

Figure 16: Partial correlations of adjacent pixels. (a) Horizontal correlation of the original image in the R channel, (b) horizontal correlation of the ciphered image in the R channel, (c) vertical correlation of the original image in the G channel, (d) vertical correlation of the ciphered image in the G channel, (e) diagonal correlation of the original image in the B channel, and (f) diagonal correlation of the ciphered image in the B channel.

Table 5: Comparison of correlation coefficients.

Correlation	Lena	Encryption image
Horizontal	0.97892	0.02025
Vertical	0.98861	0.00243
Diagonal	0.96279	−0.03036

Table 6: Information entropy comparison.

Image	Lena	Literature [37]	Literature [38]	Literature [39]	Literature [40]	Literature [41]	This study
Information entropy	6.9951	7.9974	7.9970	7.9979	7.9982	7.9989	7.9994

Figure 17: Decryption images. (a) Correct key decryption image, and (b) decrypted images with a small change in y (0).

field can also be reflected in other fields such as fault detection and secure communication. This will give chaos control practical application value and has the necessity of further development research.

8. Conclusions

A family of fourth-order chaotic systems with an infinite equilibrium point is proposed in this study. A chaotic system is selected for theoretical analysis and numerical simulation of the Lyapunov exponents spectrum, Poincarè cross section, and bifurcation diagram; the results support that the chaotic system has more complex dynamic characteristics. A circuit schematic diagram is built to verify the circuit stability and realizability of the proposed system. The parameter self-adaptive synchronization of the chaotic system is designed. The simulation results show that the synchronization control of the two systems is realized and the synchronization effects work well. The color image encryption algorithm is designed by using chaotic system synchronization control combined with DNA coding and operating rules. The histogram, information entropy, correlation coefficient of each channel, and key sensitivity are analyzed. Comparing the reference for image encryption algorithms, it is found that the algorithm has a more secure performance.

Data Availability

No data were used to support this study.

Conflicts of Interest

The authors declare that they have no conflicts of interest.

References

[1] E. Lorenz, "Deterministic nonperiodic flows," *Journal of the Atmospheric Sciences*, vol. 20, pp. 267–285, 1963.

[2] L. Yuan, C. Wang, and H. He, "A simple multi-scroll chaotic oscillator employing CCIIs[J]," *Optik - International Journal for Light and Electron Optics*, vol. 126, no. 7-8, 2015.

[3] R. Li and W. Li, "Suppressing chaos for a class of fractional-order chaotic systems by adaptive integer-order and fractional-order feedback control," *Optik - International Journal for Light and Electron Optics*, vol. 126, no. 21, 2015.

[4] H. Zhao and Q. Lai, "Complex dynamics of a new three-dimensional chaotic system," *Journal of Huazhong Normal University(Natural Sciences)*, vol. 51, no. 2, pp. 155–161, 2017, in Chinese.

[5] V.-T. Pham, S. Jafari, and C. Volos, "A novel chaotic system with heart-shaped equilibrium and its circuital implementation," *Optik - International Journal for Light and Electron Optics*, vol. 131, 2017.

[6] H. Liu, A. Kadir, and Y. Li, "Audio encryption scheme by confusion and diffusion based on multi-scroll chaotic system and one-time keys," *Optik - International Journal for Light and Electron Optics*, vol. 127, no. 19, 2016.

[7] B. Wang, S. Zhou, X. Zheng, C. Zhou, J. Dong, and L. Zhao, "Image watermarking using chaotic map and DNA coding," *Optik - International Journal for Light and Electron Optics*, vol. 126, no. 24, 2015.

[8] S. Çiçek, A. Ferikoğlu, and İ. Pehlivan, "A new 3D chaotic system: dynamical analysis, electronic circuit design, active control synchronization and chaotic masking communication application," *Optik - International Journal for Light and Electron Optics*, vol. 127, no. 8, 2016.

[9] T. Gotthans, J. Clinton Sprott, and J. Petrzela, "Simple chaotic flow with circle and square equilibrium," *International Journal of Bifurcation and Chaos*, vol. 26, no. 8, 2016.

[10] S. Aceng, V. Sundarapandian, M. Mustafa, and M. A. Muhammad, W. S. Mada Sanjaya, A new chaotic system with a pear-shaped equilibrium and its circuit simulation," *International Journal of Electrical and Computer Engineering*, vol. 8, no. 6, 2018.

[11] S. Vaidyanathan, A. Sambas, S. Kacar, and Ü. Çavuşoğlu, "A new three-dimensional chaotic system with a cloud-shaped curve of equilibrium points, its circuit implementation and sound encryption," *International Journal of Modelling, Identification and Control*, vol. 30, no. 3, 2018.

[12] V. V. Huynh, A. J. M. Khalaf, A. Alsaedi, T. Hayat, and H. R. Abdolmohammadi, "A new memristive chaotic flow with a line of equilibria," *The European Physical Journal - Special Topics*, vol. 228, no. 10, 2019.

[13] Y.-M. Yang, S.-Q. Chen, and Q. Li, "A novel hyperchaotic attractor and its application in image encryption," *Mathematics in Practice and Theory*, vol. 50, no. 21, pp. 117–125, 2020, in Chinese.

[14] S. Mobayen, S. Vaidyanathan, A. Sambas, S. Kaçar, and Ü. Çavuşoğlu, "A novel chaotic system with boomerang-shaped equilibrium, its circuit implementation and application to sound encryption," *Iranian Journal of Science and Technology, Transactions of Electrical Engineering*, vol. 43, no. 1, 2019.

[15] G. Li and Z. Bo, "A novel weak signal detection method via chaotic synchronization using chua's circuit," *IEEE Transactions on Industrial Electronics*, vol. 64, no. 3, p. 1, 2016.

[16] X.-Y. Wang, Y.-Q. Zhang, and X.-M. Bao, "A novel chaotic image encryption scheme using DNA sequence operations," *Optics and Lasers in Engineering*, vol. 73, pp. 53–61, 2015.

[17] O. U. Guocheng and X. Liu, "Four-dimensional hyperchaotic system and its application in data encryption," *Journal of Nanchang University*, vol. 42, no. 3, pp. 289–293+299, 2020, in Chinese.

[18] R. Reza, M. Saleh, F. Afef, and J. S. Ro, "Robust passivity cascade technique-based control using RBFN approximators for the stabilization of a cart inverted pendulum," *Mathematics*, vol. 9, no. 11, 2021.

[19] S. M. Esmaeilzadeh, M. Golestani, and S. Mobayen, "Chattering-free fault-tolerant attitude control with fast fixed-time convergence for flexible spacecraft," *International Journal of Control, Automation and Systems*, vol. 19, 2020.

[20] Z. Man, J. Li, X. Di, Y. Sheng, and Z. Liu, "Double image encryption algorithm based on neural network and chaos," *Chaos, Solitons & Fractals: The Interdisciplinary Journal of Nonlinear Science, and Nonequilibrium and Complex Phenomena*, vol. 152, 2021.

[21] R. Huang, K. H. Rhee, and S. Uchida, "A parallel image encryption method based on compressive sensing," *Multimedia Tools and Applications*, vol. 72, no. 1, 2014.

[22] S. Zhang and L. Liu, "A novel image encryption algorithm based on SPWLCM and DNA coding," *Mathematics and Computers in Simulation*, vol. 190, 2021.

[23] X Changbiao, G Taotao, Z De, and X Cheng, "A novel unified chaotic system and its synchronization control," *Journal of*

Nanchang University, vol. 32, no. 4, pp. 611–619, 2020, in Chinese.

[24] X.-Q. Fu, B.-C. Liu, Y.-Y. Xie, W. Li, and Y. Liu, "Image encryption-then-transmission using DNA encryption algorithm and the double chaos," *IEEE Photonics Journal*, vol. 10, p. 1, 2018.

[25] A. M. González-Zapata, E. Tlelo-Cuautle, I. Cruz-Vega, and W. D. León-Salas, "Synchronization of chaotic artificial neurons and its application to secure image transmission under MQTT for IoT protocol," *Nonlinear Dynamics*, vol. 104, 2021.

[26] I. Ahmad, M. Shafiq, and M. Mossa Al-Sawalha, "Globally exponential multi switching-combination synchronization control of chaotic systems for secure communications," *Chinese Journal of Physics*, vol. 56, no. 3, 2018.

[27] J. Luo, Z. Xiong, and S. Qu, "Adaptive multi-switching synchronization of high-order memristor-based hyperchaotic system with unknown parameters and its application in secure communication," *Complexity*, vol. 2019, Article ID 3827201, 18 pages, 2019.

[28] J. C. Sprott, "A proposed standard for the publication OF new chaotic systems," *International Journal of Bifurcation and Chaos*, vol. 21, no. 9, 2011.

[29] A. Wolf, B. Swift Jack, L. Swinney Harry, and A. Vastano John, "Determining Lyapunov exponents from a time series," *Physica D: Nonlinear Phenomena*, vol. 16, no. 3, 1985.

[30] C. Ma, J. Mou, Li Xiong, S. Banerjee, T. Liu, and X. Han, "Dynamical analysis of a new chaotic system: asymmetric multistability, offset boosting control and circuit realization," *Nonlinear Dynamics*, vol. 103, 2021.

[31] A. Khan and M. Shikha, "Dynamical behavior and reduced-order combination synchronization of a novel chaotic system," *International Journal of Dynamics and Control*, vol. 6, no. 3, 2018.

[32] A. Khan and M. Shikha, "Combination synchronization of Genesio time delay chaotic system via robust adaptive sliding mode control," *International Journal of Dynamics and Control*, vol. 6, no. 2, 2018.

[33] L. Qingdu, Z. Hongzheng, and J. Li, "Hyperchaos in a 4D memristive circuit with infinitely many stable equilibria," *Nonlinear Dynamics*, vol. 79, 2015.

[34] X. Wang, V.-T. Pham, and C. Volos, "Dynamics, circuit design, and synchronization of a new chaotic system with closed curve equilibrium," *Complexity*, Article ID 7138971, 9 pages, 2017.

[35] K. Hamede, M. Saleh, L. Marzieh, B. Farhad, and A. Chang, "LMI-Observer-Based stabilizer for chaotic systems in the existence of a nonlinear function and perturbation," *Mathematics*, vol. 9, no. 10, 2021.

[36] C. Xu, J. Sun, and C. Wang, "A novel image encryption algorithm based on bit-plane matrix rotation and hyper chaotic systems," *Multimedia Tools and Applications: International Journal*, vol. 79, no. 6, 2020.

[37] G. Ye, C. Pan, X. Huang, and Q. Mei, "An efficient pixel-level chaotic image encryption algorithm," *Nonlinear Dynamics*, vol. 94, no. 1, 2018.

[38] X. Wang, L. Liu, and Y. Zhang, "A novel chaotic block image encryption algorithm based on dynamic random growth technique," *Optics and Lasers in Engineering*, vol. 66, 2015.

[39] L. Liu and S. Miao, "A new simple one-dimensional chaotic map and its application for image encryption," *Multimedia Tools and Applications*, vol. 77, no. 16, 2018.

[40] B. Vaseghi, S. Mobayen, S. S. Hashemi, and A. Fekih, "Fast reaching finite time synchronization approach for chaotic systems with application in medical image encryption," *IEEE Access*, vol. 9, no. 99, p. 1, 2021.

[41] X. J. Tong, Z. Wang, M. Zhang, Y. Liu, H. Xu, and J. Ma, "An image encryption algorithm based on the perturbed high-dimensional chaotic map," *Springer Netherlands*, vol. 80, no. 3, 2015.